ELSEVIER

International Journal of Heat and Fluid Flow 21 (2000) 740–746

International Journal of
HEAT AND
FLUID FLOW

www.elsevier.com/locate/ijhff

Unsteady laminar hydromagnetic fluid–particle flow and heat transfer in channels and circular pipes

Ali J. Chamkha

Department of Mechanical and Industrial Engineering, College of Engineering and Petroleum, Kuwait University, P.O. Box 5969, 13060 Safat, Kuwait

Received 15 October 1998; accepted 4 April 2000

Abstract

The problem of unsteady laminar flow and heat transfer of a particulate suspension in an electrically conducting fluid through channels and circular pipes in the presence of a uniform transverse magnetic field is formulated using a two-phase continuum model. Two different applied pressure gradient (oscillating and ramp) cases are considered. The general governing equations of motions (which include such effects as particulate phase stresses, magnetic force, and finite particle-phase volume fraction) are non-dimensionalized and solved in closed form in terms of Fourier cosine and Bessel functions and the energy equations for both phases are solved numerically since they are non-linear and are difficult to solve analytically. Numerical solutions based on the finite-difference methodology are obtained and graphical results for the fluid-phase volumetric flow rate, the particle-phase volumetric flow rate, the fluid-phase skin-friction coefficient and the particle-phase skin-friction coefficient as well as the wall heat transfer for plane and axisymmetric flows are presented and discussed. In addition, these numerical results are validated by favorable comparisons with the closed-form solutions. A comprehensive parametric study is performed to show the effects of the Hartmann magnetic number, the particle loading, the viscosity ratio, and the temperature inverse Stokes number on the solutions.

1. Introduction

The importance and application of solid/fluid flows and heat transfer in petroleum transport, wastewater treatment, combustion, power plant piping, corrosive particles in engine oil flow, and many others are well known in the literature. Particularly, the flow and heat transfer of electrically conducting fluids in channels and circular pipes under the effect of a transverse magnetic field occurs in magnetohydrodynamic (MHD) generators, pumps, accelerators, and flowmeters and has possible applications in nuclear reactors, filtration, geothermal systems, and others. The possible presence of solid particles such as ash or soot in combustion MHD generators and plasma MHD accelerators and their effect on the performance of such devices led to studies of particulate suspensions in conducting fluids in the presence of magnetic fields. For example, in an MHD generator, coal mixed with seed is fed into a combustor. The coal and seed mixture is burned in oxygen and the combustion gas expands through a nozzle before it enters the generator section. The gas mixture flowing through the MHD channel consists of a condensable vapor (slag) and a non-condensable gas mixed with seeded coal combustion products. Both the slag and the non-condensable gas are electrically conducting (see, Loharsbi, 1980). The presence of the slag and the seeded coal particles significantly influences the flow and heat transfer characteristics in the MHD channel. Ignoring the effect of the slag, and considering the MHD generator start-up condition, the problem reduces to unsteady two-phase flow in an MHD channel.

In general, there are two basic approaches to model two-phase fluid/particle flows. These are based on the Eulerian and Lagrangian descriptions known from fluid mechanics. The former treats both the fluid- and the particle-phases as interacting continua (see, for instance, Marble, 1970) while the latter treats only the fluid-phase as continuum with the particle-phase being governed by the kinetic theory (see Berlemont et al., 1990). The present work employs the continuum approach and uses a modified dusty-gas model to include particle-phase viscous stresses, finite particle volume fraction, and a hydromagnetic body force.

The particle-phase viscous stresses can be used to model particle–particle interaction. They can be thought of as a natural consequence of the averaging processes employed to model a discrete system of particles as a continuum (see, for instance, Drew and Segal, 1971; Drew, 1983). Previously published work which includes the particle-phase viscous stresses can be found in the papers by Gidaspow (1986), Tsuo and Gidaspow (1990), and Gadiraju et al. (1992). In the present work, both the fluid- and the particle-phases are assumed to be incompressible and have constant properties, and the particle-phase volume fraction is assumed to be constant and finite. In reality, the particle-phase volume fraction is non-

E-mail address: chamkha@kuc01.kuniv.edu.kw (A.J. Chamkha).

0142-727X/00/$ - see front matter
PII: S0142-727X(00)00031-X

Notation

a	pipe radius or channel half width
B_0	magnetic induction
c	fluid-phase specific heat
C	fluid-phase skin-friction coefficient defined in Eq. (7)
c_p	particle-phase specific heat
C_p	particle-phase skin-friction coefficient defined in Eq. (7)
Ec	Eckert number, $(G_0a^2/\mu)^2/(cT_1)$
F	dimensionless fluid-phase velocity, $Vl/(G_0a^2/\mu)$
F_p	dimensionless particle-phase velocity, $Vp/(G_0a^2/\mu)$
G	dimensionless pressure gradient, $-1/G_0\ \partial P/\partial z$
J_1	first-order Bessel function of the first kind
J_0	zeroth-order Bessel function of the first kind
k	fluid thermal conductivity
M	Hartmann number, $\sqrt{\sigma/\mu}B_0a$
P	pressure
Pr	Prandtl number, $\mu c/k$
Q	fluid-phase volumetric flow rate defined in Eq. (7)
Q_p	particle-phase volumetric flow rate defined in Eq. (7)
q_w	wall heat flux defined in Eq. (7)
r	distance in the radial direction
t	time
T	fluid-phase temperature
T_0	fluid-phase wall temperature
T_p	particle-phase temperature
V	fluid-phase velocity
V_p	particle-phase velocity
z	axial direction

Greeks

x	momentum inverse Stokes number, $a^2\rho/(\mu\tau_v)$
β	viscosity ratio, μ_p/μ
ε	temperature inverse Stokes number, $a^2\rho/(\mu\tau_T)$
ϕ	particle-phase volume fraction
γ	specific heat ratio, c_p/c
η	dimensionless radial distance, r/a
κ	particle loading, $\rho_p\ \phi/(\rho(1-\phi))$
λ_m, λ_n	eigenvalues
μ	fluid-phase dynamic viscosity
μ_p	particle-phase dynamic viscosity
θ	dimensionless fluid-phase temperature, T/T_0
θ_p	dimensionless particle-phase temperature, T_p/T_0
ρ	fluid-phase density
ρ_p	particle-phase density
σ	fluid electrical conductivity
τ	dimensionless time, $t/(a^2\rho/\mu)$
τ_0	reference dimensionless time
τ_t	temperature relaxation time
τ_v	momentum relaxation time
ω	circular frequency of oscillation

uniform but it is assumed to be constant herein so as to allow the governing equations to be solved analytically. In order to model many situations, multiphase (fluid–particle) theories will eventually need to allow for a transition of the particle-phase from fluid-like behavior at low volume fraction to solid-like behavior at large volume fraction. The inclusion of a particle-phase viscosity as a function of the volume fraction represents a step in that direction (Gadiraju et al., 1992). It should be noted that if the particle-phase viscosity is allowed to increase rapidly with the volume fraction, the particle-phase will behave as a rigid body at large values of the volume fraction. This is not done herein and the particle-phase viscosity is assumed to be constant in order to obtain closed-form solutions. However, there have been some published works which predict variable particle-phase volume fraction (see, for instance, Soo, 1969; Sinclair and Jackson, 1989; Drew and Lahey, 1982). The inclusion of a lift force in the governing equations is sufficient (but not necessary) to produce non-uniform volume fraction distribution. In addition, as a result of the inclusion of the particle-phase viscous stresses, the particle-phase will have a corresponding pressure. This pressure will be constant for uniform particle-phase volume fraction situations and, therefore, the particle-phase pressure gradient will vanish.

The single-phase flow of conducting fluids in pipes with circular cross-sections has been investigated by many authors (see, for instance, Shercliff, 1956; Gold, 1962). Tseng and Sahai (1982) reported solutions for steady MHD flow of a suspension in pipes. Dube and Sharma (1975) and Ritter and Peddieson (1977) reported solutions for unsteady dusty-gas flow in a circular pipe in the absence of a magnetic field. Related work on channel flow can be found in the thesis by Ritter (1976), the papers by Mitra and Bhattacharya (1981) and Chamkha (1995a, 1995b), and the book by White (1991). The purpose of this paper is to obtain closed-form transient solutions for hydromagnetic two-phase particulate suspension flow in channels and circular pipes and numerical solutions for the thermal problem. This will be done for both oscillating and ramp pressure gradients applied along the flow direction.

2. Governing equations

Consider unsteady, laminar, hydromagnetic, fully developed, plane and axisymmetric flow of a particle/fluid suspension in a horizontal channel or a circular pipe due to the action of an arbitrary time-varying pressure gradient. A uniform transverse magnetic field is applied normal to the flow direction (see Fig. 1). The fluid-phase is assumed to be electrically conducting while the particle-phase and the pipe or channel walls are assumed to be electrically non-conducting. No electric field is assumed to exist and the magnetic Reynolds number is assumed to be small so that the induced magnetic field and the Hall effect of MHDs are negligible. The governing equations for this study are based on the conservation laws of mass, linear momentum and energy of both phases. In this work, it is assumed that both phases are treated as two interacting continua (see, for instance, Marble, 1970). The interaction between the phases is restricted to the interphase drag force which is modeled by Stokes linear drag theory and the interphase heat transfer. Under these assumptions, the

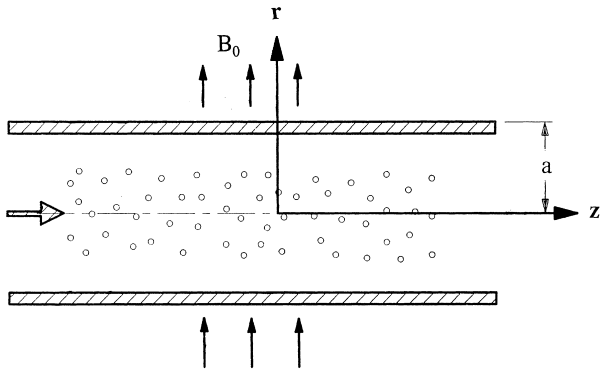

Fig. 1. Problem definition.

governing equations with $j = 0$ for plane channel flow and $j = 1$ for axisymmetric pipe flow can be written in dimensionless form as

$$\frac{\partial F}{\partial \tau} = \frac{\partial^2 F}{\partial \eta^2} + \frac{j}{\eta}\frac{\partial F}{\partial \eta} + \kappa\alpha(F_p - F) - M^2 F + G(\tau), \tag{1}$$

$$\frac{\partial F_p}{\partial \tau} = \beta\frac{\partial^2 F_p}{\partial \eta^2} + \frac{j}{\eta}\frac{\partial F_p}{\partial \eta} + \alpha(F - F_p), \tag{2}$$

$$\frac{\partial \theta}{\partial \tau} = \frac{1}{Pr}\left(\frac{\partial^2 \theta}{\partial \eta^2} + \frac{j}{\eta}\frac{\partial \theta}{\partial \eta}\right) + Ec\left(\frac{\partial F}{\partial \eta}\right)^2 + Ec\,\kappa\alpha\left(F_p - F\right)^2 + Ec\,M^2F^2 + \kappa\gamma\varepsilon\left(\theta_p - \theta\right), \tag{3}$$

$$\frac{\partial \theta_p}{\partial \tau} = \frac{\beta\, Ec}{\gamma}\left(\frac{\partial F_p}{\partial \eta}\right)^2 - \varepsilon(\theta_p - \theta), \tag{4}$$

where $\beta = \mu_p/\mu$, $\alpha = a^2\rho/(\mu\tau_v)$, $M = \sqrt{\sigma/\mu}B_0 a$, $Pr = \mu c/k$, $\gamma = c_p/c$, $Ec = (G_0 a^2/\mu)^2/(cT_1)$, $\varepsilon = a^2\rho/(\mu\tau_T)$, are the viscosity ratio, momentum inverse Stokes number, the Hartmann number, the Prandtl number, the specific heat ratio, the Eckert number, and the temperature inverse Stokes number, respectively. It should be noted that in obtaining Eqs. (1)–(4) the following non-dimensionalization parameters are employed where the meaning of the parameters is given in the Notation:

$$\begin{aligned} &r = a\eta, \quad t = a^2\rho\tau/\mu, \quad \rho_p = \kappa\rho(1-\phi)/\phi,\\ &\partial P/\partial z = -G_0 G(\tau), \quad V(r,t) = G_0 a^2/\mu\, F(\eta,\tau),\\ &V_p(r,t) = G_0 a^2/\mu\, F_p(\eta,\tau), \quad T(r,t) = T_0\theta(\eta,\tau),\\ &T_p(r,t) = T_0\theta_p(\eta,\tau). \end{aligned} \tag{5}$$

Eqs. (1)–(4) are supplemented by the following dimensionless initial and boundary conditions:

$$\begin{aligned} &F(\eta,0) = 0, \quad F_p(\eta,0) = 0, \quad F(0,\tau) \neq \infty,\\ &F_p(0,\tau) \neq \infty, \quad F(1,\tau) = 0, \quad F_p(1,\tau) = 0,\\ &\theta(\eta,0) = 0, \quad \theta_p(\eta,0) = 0, \quad \theta(0,\tau) \neq \infty,\\ &\theta_p(0,\tau) \neq \infty, \quad \theta(1,\tau) = 1. \end{aligned} \tag{6}$$

Of special interest in the present work is to observe the behaviors of the volumetric flow rates (Q and Q_p) for the fluid- and the particle-phases, the fluid- and particle-phase skin-friction coefficients (C and C_p) and the wall heat transfer (q_w) at the upper wall of the channel under various conditions. These physical parameters can, respectively, be defined taking into account the flow symmetry of the problem as follows:

$$\begin{aligned} &Q = 2\int_0^1 (\pi\eta)^\delta F(\eta,\tau)\,d\eta, \quad Q_p = 2\int_0^1 (\pi\eta)^\delta F_p(\eta,\tau)\,d\eta,\\ &C = -\frac{\partial F}{\partial \eta}(1,\tau), \quad C_p = -\beta\kappa\frac{\partial F_p}{\partial \eta}(1,\tau),\\ &q_w = \frac{-1}{Pr\,Ec}\frac{\partial \theta}{\partial \eta}(0,\tau), \quad \delta = \begin{cases} 0, & \text{for plane flow,}\\ 1, & \text{for pipe flow.}\end{cases} \end{aligned} \tag{7}$$

3. Analytical results

Eqs. (1)–(4) and (6) represent an initial-value problem. Since the flow of the suspension is assumed incompressible with constant properties, the hydrodynamic problem is uncoupled from the thermal problem. In addition, the hydrodynamic problem consisting of Eqs. (1) and (2) is linear and can be solved by the method of expansion in orthogonal functions. However, the thermal problem is non-linear and must be solved numerically. Therefore, respectively closed-form and numerical solutions for the hydrodynamic and thermal problems will be reported in this paper. The hydrodynamic solution can be obtained by assuming that the solutions for F and F_p take on the forms

$$\begin{aligned} j = 0: \quad &F(\eta,\tau) = \sum_{n=1}^{\infty} H_n(\tau)\cos(\lambda_n\eta),\\ &F_p(\eta,\tau) = \sum_{n=1}^{\infty} H_{pn}(\tau)\cos(\lambda_n\eta),\\ j = 1: \quad &F(\eta,\tau) = \sum_{n=1}^{\infty} H_n(\tau)J_0(\lambda_n\eta),\\ &F_p(\eta,\tau) = \sum_{n=1}^{\infty} H_{pn}(\tau)J_0(\lambda_n\eta), \end{aligned} \tag{8}$$

where λ_n are roots of the equation $\cos(\lambda_n\eta) = 0$ for channel flow and the equation $J_0(\lambda_n\eta) = 0$ (J_0 being the zeroth-order Bessel function of the first kind) for pipe flow and H_n and H_{pn} are functions to be determined. Substituting Eqs. (8) and their derivatives into Eqs. (1) and (2) (with the non-homogeneous part of these equations represented by a series in $\cos(\lambda_n\eta)$ for channel flow and $J_0(\lambda_n\eta)$ for pipe flow), multiplying by $\cos(\lambda_m\eta)$for channel flow and by $\eta J_0(\lambda_m\eta)$for pipe flow (to take advantage of the orthogonality property of Fourier cosine and Bessel functions), and then integrating with respect to η from 0 to 1 yield

$$\dot{H}_n + \left(\lambda_n^2 + \kappa\alpha + M^2\right)H_n - \kappa\alpha H_{pn} = b_n G(\tau), \tag{9}$$

$$\dot{H}_{pn} + \beta\lambda_n^2 H_{pn} + \alpha(H_{pn} - H_n) = 0, \tag{10}$$

where a dot denotes ordinary differentiation with respect to τ and $b_n = 2(-1)^{n+1}/\lambda_n$ for channel flow and $b_n = 2/(\lambda_n J_1(\lambda_n))$ (J_1 being the first-order Bessel function of the first kind) for pipe flow. Combining Eqs. (9) and (10) gives

$$\ddot{H}_n + \left(\lambda_n^2(1+\beta) + \alpha(1+\kappa) + M^2\right)\dot{H}_n + \left(\beta\lambda_n^2\left(M^2 + \lambda_n^2 + \kappa\alpha\right) + \alpha\left(\lambda_n^2 + M^2\right)\right)H_n = b_n\left(\dot{G}(\tau) + \left(\beta\lambda_n^2 + \alpha\right)G(\tau)\right). \tag{11}$$

It should be mentioned that analytical solutions for the case of constant pressure gradient along with their corresponding steady-state solutions were reported earlier by Chamkha (1995a) for channel flow. Therefore, the above equation will be solved only for oscillating and ramp pressure gradient conditions.

With the solutions of F and F_p (given by Eqs. (8)) known, the corresponding expressions for Q, Q_p, C and C_p can be written as

$$\begin{aligned} &Q = 2\sum_{n=1}^{\infty}(-1)^{n+1}\,H_n/\lambda_n, \quad Q_p = 2\sum_{n=1}^{\infty}(-1)^{n+1}H_{pn}/\lambda_n,\\ &C = \sum_{n=1}^{\infty}(-1)^{n+1}\lambda_n H_n, \quad C_p = \beta\kappa\sum_{n=1}^{\infty}(-1)^{n+1}\lambda_n H_{pn} \end{aligned} \tag{12}$$

for plane flow and

$$\begin{aligned} &Q = 4\pi\sum_{n=1}^{\infty}H_n/\left(b_n\lambda_n^2\right), \quad Q_p = 4\pi\sum_{n=1}^{\infty}H_{pn}/\left(b_n\lambda_n^2\right),\\ &C = 2\sum_{n=1}^{\infty}H_n/b_n, \quad C_p = 2\beta\kappa\sum_{n=1}^{\infty}H_{pn}/b_n \end{aligned} \tag{13}$$

for axisymmetric flow.

4. Oscillating pressure gradient solutions

Assuming that the pressure gradient $G(\tau)$ is a general sinusoidal function of the form

$$G(\tau) = G_s \sin(\omega\tau) + G_c \cos(\omega\tau), \tag{14}$$

where ω (a constant) is the circular frequency of oscillation, and G_s and G_c are constants and substituting into Eq. (11) results in

$$\begin{aligned}\ddot{H}_n &+ \left(\lambda_n^2(1+\beta) + \alpha(1+\kappa) + M^2\right)\dot{H}_n \\ &+ \left(\beta\lambda_n^2\left(M^2+\lambda_n^2+\kappa\alpha\right) + \alpha\left(\lambda_n^2+M^2\right)\right)H_n \\ &= b_n\left(G_s\left(\beta\lambda_n^2+\alpha\right) - G_c\omega\sin(\omega\tau)\right. \\ &\quad \left. + \left(G_c\left(\beta\lambda_n^2+\alpha\right) + G_s\omega\right)\cos(\omega\tau)\right).\end{aligned} \tag{15}$$

The general solution to the above equation can be shown to be

$$\begin{aligned}H_n &= c_3\exp(s_1\tau) + c_4\exp(s_2\tau) + c_5\sin(\omega\tau) \\ &\quad + c_6\cos(\omega\tau),\end{aligned} \tag{16}$$

where

$$c_5 = (X_1Z_1 + Y_1Z_2)/\left(X_1^2+Y_1^2\right), \quad c_6 = (X_1Z_2 + Y_1Z_1)/\left(X_1^2+Y_1^2\right),$$

$$X_1 = \beta\lambda_n^2\left(M^2+\lambda_n^2+\kappa\alpha\right) + \alpha\left(M^2+\lambda_n^2\right) - \omega^2,$$

$$Y_1 = \left(M^2 + \lambda_n^2(1+\beta) + \alpha(1+\kappa)\right)\omega,$$

$$Z_1 = b_n\left(G_s\left(\beta\lambda_n^2+\alpha\right) - G_c\omega\right), \quad Z_2 = b_n\left(G_s\left(\beta\lambda_n^2+\alpha\right) + G_c\omega\right). \tag{17}$$

Application of the initial conditions gives

$$c_4 = (c_6s_1 - c_5\omega + b_nG_c)/(s_2 - s_1), \quad c_3 = -c_4 - c_6. \tag{18}$$

For this case the appropriate solution for H_{pn} takes on the form

$$\begin{aligned}H_{pn} &= 1/(\kappa\alpha)\left(c_1\left(s_1+\lambda_n^2+\kappa\alpha+M^2\right)\exp(s_1\tau)\right. \\ &\quad + c_2\left(s_2+\lambda_n^2+\kappa\alpha+M^2\right)\exp(s_2\tau) \\ &\quad + \left(c_5\omega + c_6\left(M^2+\lambda_n^2+\kappa\alpha\right) - b_nG_c\right)\cos(\omega\tau) \\ &\quad \left. + \left(c_5\left(M^2+\lambda_n^2+\kappa\alpha\right) - c_6\omega - b_nG_s\right)\sin(\omega\tau)\right).\end{aligned} \tag{19}$$

The above analytical solutions are consistent with the solutions for the special cases reported earlier by Ritter (1976) and Chamkha (1995b).

5. Ramp pressure gradient solutions

For this special case, the pressure gradient $G(\tau)$ is assumed to take on the form

$$G(\tau) = \begin{cases} \tau/\tau_0, & \tau < \tau_0, \\ 1, & \tau \geqslant \tau_0. \end{cases} \tag{20}$$

In this case, it is needed to consider both ranges when $\tau < \tau_0$ and $\tau \geqslant \tau_0$. Similar to the previous case of oscillating pressure gradient, the expression for $G(\tau)$ in the different ranges is substituted into Eq. (11) and solved by subjecting to the initial conditions. It should be mentioned that the condition of continuity of solutions must be ensured at $\tau = \tau_0$. Without going into the details, it can be shown that the solutions for H_n and H_{pn} for this case can be written as

$$H_n = \begin{cases} c_7\exp(s_1\tau) + c_8\exp(s_2\tau) + A_1 + B_1\tau, & \tau < \tau_0, \\ R\exp(s_1\tau) + S\exp(s_2\tau) + Z, & \tau \geqslant \tau_0, \end{cases} \tag{21}$$

$$H_{pn} = \begin{cases} 1/(\kappa\alpha)c_7\left(s_1+M^2+\lambda_n^2+\kappa\alpha\right)\exp(s_1\tau) \\ \quad + c_8\left(s_1+M^2+\lambda_n^2+\kappa\alpha\right)\exp(s_2\tau) + B_1 \\ \quad + \left(M^2+\lambda_n^2+\kappa\alpha\right)(A_1+B_1\tau) - b_n\tau/\tau_0, & \tau < \tau_0, \\ 1/(\kappa\alpha)\left(R\left(s_1+M^2+\lambda_n^2+\kappa\alpha\right)\exp(s_1\tau)\right. \\ \quad + S\left(s_2+M^2+\lambda_n^2+\kappa\alpha\right)\exp(s_2\tau) \\ \quad \left. + Z\left(M^2+\lambda_n^2+\kappa\alpha\right) - b_n\right), & \tau \geqslant \tau_0, \end{cases} \tag{22}$$

where

$$R = \left(b_n + \kappa\alpha Y + s_2Z - X\left(s_2+M^2+\lambda_n^2+\kappa\alpha\right)\right) \Big/ \left((s_1-s_2)\exp(s_1\tau_0)\right), \tag{23}$$

$$S = \left(b_n + \kappa\alpha Y + s_1Z - X\left(s_1+M^2+\lambda_n^2+\kappa\alpha\right)\right) \Big/ \left((s_2-s_1)\exp(s_2\tau_0)\right), \tag{24}$$

$$Z = b_n\left(\beta\lambda_n^2+\alpha\right)/\left(\beta\lambda_n^2\left(M^2+\lambda_n^2+\kappa\alpha\right) + \alpha\left(M^2+\lambda_n^2\right)\right), \tag{25}$$

$$\begin{aligned}X &= c_7\exp(s_1\tau_0) + c_8\exp(s_2\tau_0) + A_1 + B_1\tau_0, \\ Y &= 1/(\kappa\alpha)\left(c_7\left(s_1+M^2+\lambda_n^2+\kappa\alpha\right)\exp(s_1\tau_0)\right. \\ &\quad + c_8\left(s_2+M^2+\lambda_n^2+\kappa\alpha\right)\exp(s_2\tau_0) \\ &\quad \left. + (A_1+B_1\tau_0)\left(M^2+\lambda_n^2+\kappa\alpha\right) + B_1 - b_n\right),\end{aligned} \tag{26}$$

$$\begin{aligned}A_1 &= \left(b_n/\tau_0 - B_1\left(M^2+\lambda_n^2(1+\beta)\right.\right. \\ &\quad \left.\left. + \alpha(1+\kappa)\right)\right)/\left(\beta\lambda_n^2\left(M^2+\lambda_n^2+\kappa\alpha\right) + \alpha\left(M^2+\lambda_n^2\right)\right), \\ B_1 &= b_n\left(\beta\lambda_n^2+\alpha\right)/\left(\tau_0\left(\beta\lambda_n^2\left(M^2+\lambda_n^2+\kappa\alpha\right) + \alpha\left(M^2+\lambda_n^2\right)\right)\right),\end{aligned} \tag{27}$$

$$c_7 = (A_1s_2 - B_1)/(s_1 - s_2), \quad c_8 = (A_1s_1 - B_1)/(s_2 - s_1). \tag{28}$$

It should be mentioned that if both of β and M are formally set to 0 in Eqs. (20)–(28), the results reported by Ritter (1976) for a ramp pressure gradient are recovered.

6. Numerical results

The general physical effects of the various parameters on the solutions of the oscillating pressure gradient case are similar to those associated with the ramp pressure gradient case. For this reason, attention will be focused on the latter case. A representative set of hydrodynamic and thermal results is given below for both channel and pipe flows in the presence of combined particle-phase viscosity and magnetic effects. All subsequent results are obtained numerically using the finite-difference methodology. The method employed is implicit and iterative. Constant step sizes of 0.01 are used in the radial direction and variable step sizes in time with an initial time step of 0.01 and a growth factor of 1.02. These values are arrived at after much numerical experimentation was performed to assess grid independence. For example, when $\Delta\eta$ was set to 0.001, no significant changes in results were observed in which the error was only about 1%. In addition, when constant step sizes in τ were used, an average error of less than 2% was predicted. The solution convergence criterion was based on the difference between the current and the previous iterations and convergence was assumed to achieve when this difference reached 10^{-5}. The numerical flow solutions were checked against the analytical results given in Eqs. (20)–(28) and were found to be in excellent agreement. A representative comparison between the numerical and analytical results for Q, Q_p, C, and C_p is shown in Figs. 2–5. It should be mentioned that in the

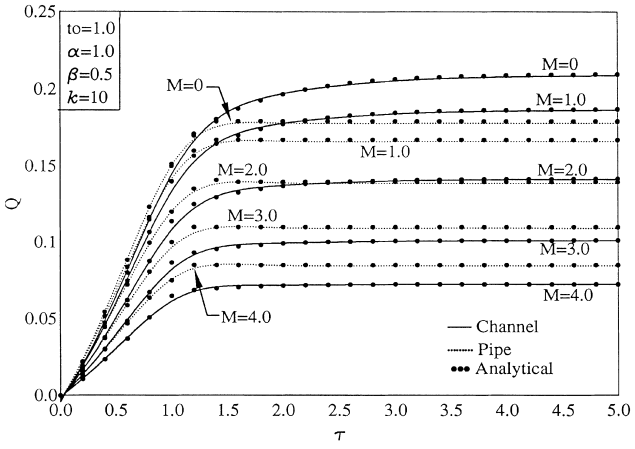

Fig. 2. Effects of M on fluid-phase volume flow rate time history.

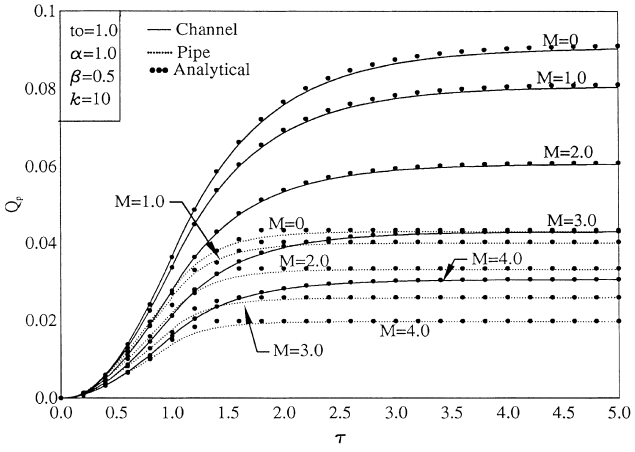

Fig. 3. Effects of M on particle-phase volume flow rate time history.

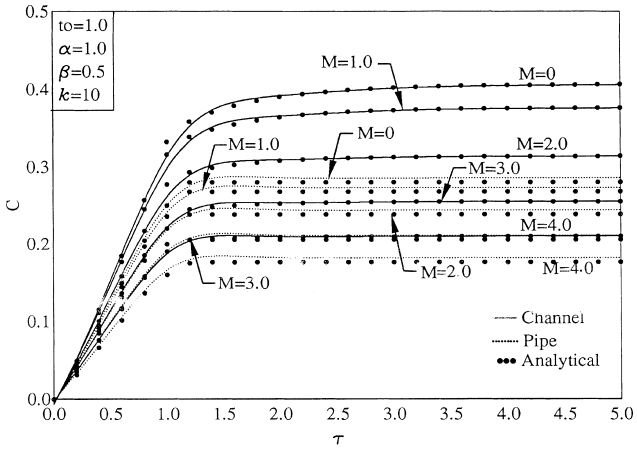

Fig. 4. Effects of M on fluid-phase skin-friction coefficient time history.

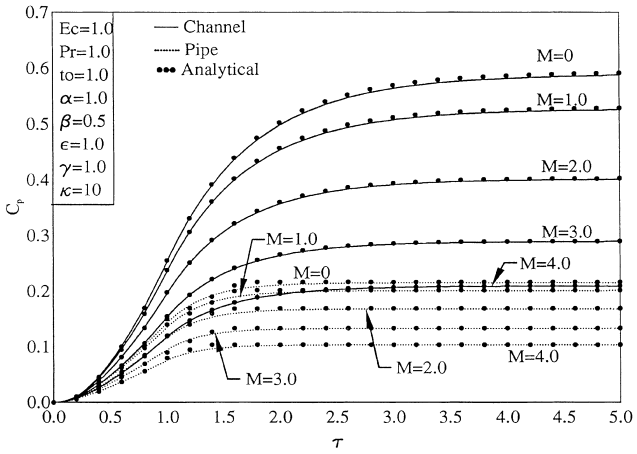

Fig. 5. Effects of M on particle-phase skin-friction coefficient time history.

numerical evaluation of the analytical solutions, 50 terms of the series were used.

Figs. 2–5 present typical time histories for the fluid-phase volume flow rate Q, particle-phase volume flow rate Q_p, fluid-phase skin-friction coefficient C, and the particle-phase skin-friction coefficient C_p for both channel and pipe flow situations and various values of the Hartmann number M based on both the numerical and analytical solutions, respectively. Imposition of a magnetic field normal to the flow direction gives rise to a drag-like or resistive force in the direction of flow. This force is called the Lorentz force and it has the tendency to slow down or suppress the movement of the fluid in the channel or pipe, which in turn reduces the motion of the suspended particle-phase. This is translated into reductions in the average velocities of both the fluid- and the particle-phases and, consequently, in their flow rates. In addition, the reduced motion of the particulate suspension in the channel or pipe as a result of increasing the strength of the magnetic field causes lower velocity gradients at the wall. This has the direct effect of reducing the skin-friction coefficients of both phases. These and the previous behaviors are clearly evident in the decrease of Q, Q_p, C, and C_p as M increases as shown in Fig. 2, 3, 4 and 5, respectively. Furthermore, it is also observed from these figures that, in general, lower values of Q, Q_p, C, and C_p are predicted for the case of pipe flow than for the case of channel flow at the same conditions with the exception of Q for relatively large values of M ($M > 3$). The excellent agreement between the numerical and analytical solutions for all of the conditions considered is also apparent in these figures.

The effects of the particle loading parameter κ on transient channel and pipe flow and heat transfer results for Q, Q_p, C, C_p and q_w were obtained but not presented herein for brevity. Similar to the magnetic field effect, increases in the particle loading or particle concentration in the channel or pipe cause the movement of the fluid and the particles to be slower which results in reductions in Q, Q_p, and C and increases in the values of C_p since it is directly proportional to κ (see definition of C_p). These behaviors were consistent with the obtained results. Also, the effect of increasing κ was found to decrease the steady-state profiles of the fluid-phase temperature θ and the particle-phase temperature θ_p. This decrease in temperature is due to the decrease in the velocity distribution caused by increase in the particle loading. However, the wall gradients of the fluid temperature profiles was predicted to increase as κ increased for all times. This caused the wall heat transfer q_w to increase as κ was increased for all times.

Figs. 6 and 7 display the variations in the values of C and C_p that are brought about by changes in the viscosity ratio β as the flow time progresses from non-steady to steady-state conditions, respectively. Endowing the particle-phase with an artificial viscosity has been shown to be especially valid for dense suspensions (see, Gidaspow, 1986; Tsuo and Gidaspow, 1990).

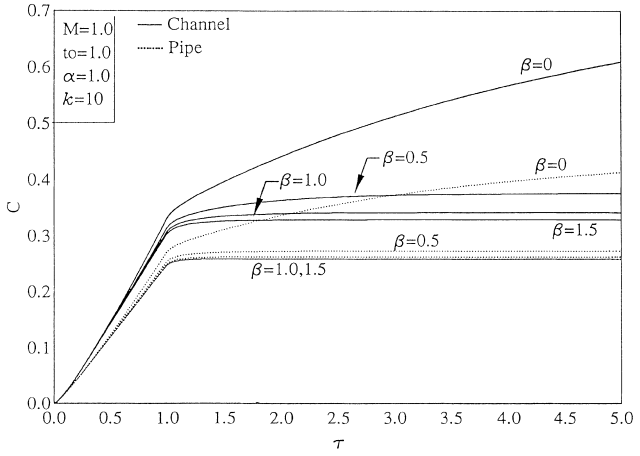

Fig. 6. Effects of β on fluid-phase skin-friction coefficient time history.

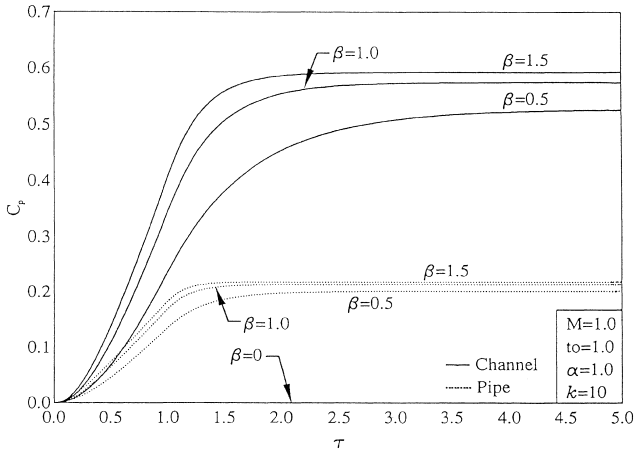

Fig. 7. Effects of β on particle-phase skin-friction coefficient time history.

In these situations, as the particle-phase viscosity coefficient μ_p increases (that is, β increases), the suspension becomes more viscous and will be moving with an effective viscosity $\mu + \mu_p$. This will represent the case of high particle concentration. Therefore, as β increases, the flow rates of both phases as well as the fluid-phase wall friction decreases considerably. However, since C_p is defined as directly proportional to β, it increases as β increases at all times. These facts are evident from Figs. 6 and 7. Also, the wall heat transfer is observed to be unaffected by changes in β. In addition, it is noted that the changes in the flow characteristics of both phases for $\beta > 1$ are not as great as for $0 \leqslant \beta \leqslant 1$. Again, the flow and heat transfer characteristics for pipe flow are lower than those associated with channel flow at the same conditions.

It is also observed from other results not presented herein that increasing the Eckert number produces significantly higher steady-state temperature distributions for both the fluid- and the particle-phases. Also, increasing the fluid Prandtl number Pr causes the steady-state temperature profiles θ and θ_p as well as the wall heat transfer q_w to decrease. In addition, contrary to the cases discussed before, the pipe flow results for θ and θ_p are found to be higher than those corresponding to channel flow at the same conditions.

The effects of the temperature inverse Stokes number ε on the temperature profiles θ and θ_p and the transient distribution of q_w are presented in Fig. 8, 9 and 10, respectively. Increases in the values of ε increase the thermal coupling or energy transfer between the fluid- and the particle-phases. This causes the fluid-phase temperature to decrease and the particle-phase temperature to increase as clearly shown in

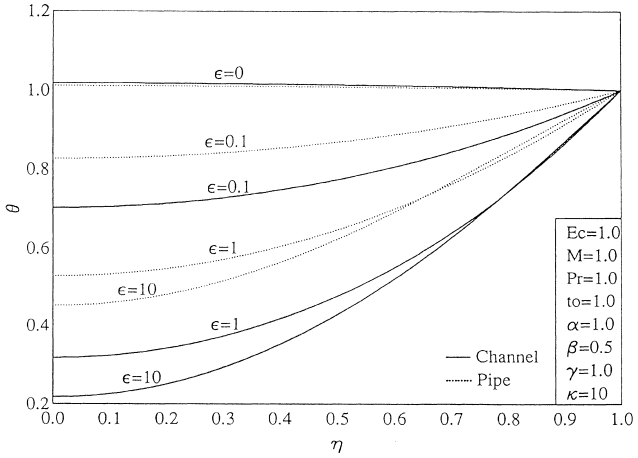

Fig. 8. Effects of ε on the fluid-phase temperature profiles.

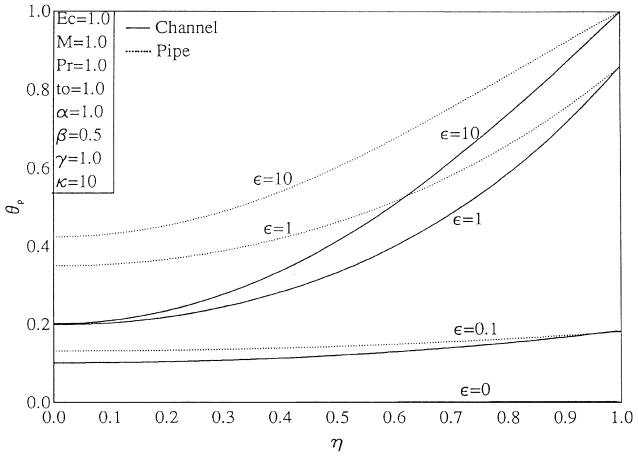

Fig. 9. Effects of ε on the particle-phase temperature profiles.

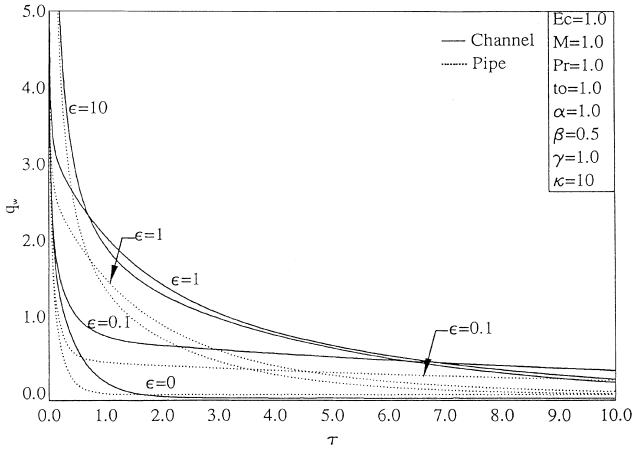

Fig. 10. Effects of ε on wall heat transfer coefficient time history.

Figs. 8 and 9, respectively. The particle-phase wall temperature is not prescribed since the particle-phase energy equation is a first-order differential equation and, therefore, it is adjusted through the thermal coupling process. The wall heat transfer q_w is dependent on the slope of the fluid-phase temperature at the wall which increases as ε increases. This results in increasing the wall heat transfer as shown in Fig. 10.

7. Conclusion

In this paper, the transient flow and heat transfer of a particulate suspension in an electrically conducting fluid in a channel and a circular pipe with an applied transverse magnetic field was studied for the cases of both oscillating and ramp pressure gradients. The governing equations for this investigation were derived, non-dimensionalized, and solved analytically and numerically. The analytical solutions were obtained for the hydrodynamic or flow problem while the thermal problem was solved numerically using an implicit finite-difference method. Numerical evaluations of the exact solutions were performed and successfully compared with the fully numerical solutions. Graphical results for the fluid-phase volumetric flow rate, the particle-phase volumetric flow rate, the fluid-phase skin-friction coefficient, and the particle-phase skin-friction coefficient are presented and discussed to show the effects of the Hartmann magnetic number, the particle loading, and the viscosity ratio on the solutions. In addition, finite-difference solutions of the energy equations of both phases were performed and graphical results were presented to show the influence of the temperature inverse Stokes number on the temperature profiles of both phases and the wall heat transfer. While favorable comparisons with previously published theoretical work on this problem are performed, no experimental data were found to check the validity of the assumptions made. It is hoped that the results reported herein will serve as a check for further theoretical modeling and a stimulus for experimental work on this problem.

Acknowledgements

The author acknowledges and is greatful for the financial support of the Research Administration at Kuwait University through the Research Project EPM-082.

References

Berlemont, A., Desjonqueres, P., Gouesbet, G., 1990. Particle Lagrangian simulation in turbulent flows. Int. J. Multiphase Flow 16, 19–34.

Chamkha, A.J., 1995a. Hydromagnetic two-phase flow in a channel. Int. J. Eng. Sci. 33, 437–446.

Chamkha, A.J., 1995b. Time dependent two-phase channel flow due to an oscillating pressure gradient. Fluid/Particle Separation J. 8, 196–203.

Drew, D.A., 1983. Mathematical modeling of two-phase flow. Ann. Rev. Fluid Mech. 15, 261–291.

Drew, D.A., Segal, L.A., 1971. Analysis of fluidized beds and foams using averaged equations. Stud. Appl. Math. 50, 233–252.

Drew, D., Lahey, R.T., 1982. Phase distribution mechanisms in turbulent two-phase flow in a circular pipe. J. Fluid Mech. 117, 91–106.

Dube, S.N., Sharma, C.L., 1975. A note on unsteady flow of a dusty viscous liquid in a circular pipe. J. Phys. Soc. Jpn 38 (1), 298.

Gadiraju, M., Peddieson, J., Munukutla, S., 1992. Exact solutions for two-phase vertical pipe flow. Mech. Res. Commun. 19, 7–13.

Gidaspow, D., 1986. Hydrodynamics of fluidization and heat transfer: super computer modeling. Appl. Mech. Rev. 39, 1–23.

Gold, R.R., 1962. Magnetohydrodynamic pipe flow. Part I. J. Fluid Mech. 13 (4), 505–512.

Lohrasbi, J., 1980. Investigation of magnetohydrodynamic heat transfer in two-phase flow. Ph.D. Thesis, Tennessee Technological University, p. 1.

Marble, F.E., 1970. Dynamics of dusty gases. Ann. Rev. Fluid Mech. 2, 397–446.

Mitra, P., Bhattacharya, P., 1981. On the hydromagnetic flow of a dusty fluid between two-parallel plates, one being stationary and the other oscillating. J. Phys. Soc. Jpn 50, 995–1001.

Ritter, J.M., 1976. Two phase fluid flow in pipes and channels. M.S. Thesis, Tennessee Technological University.

Ritter, J.M., Peddieson, J., 1977. Transient two-phase flows in channels and circular pipes. In: Proceeding of the Sixth Canadian Congress of Applied Mechanics.

Shercliff, J.A., 1956. The flow of conducting fluids in circular pipes under transverse magnetic fields. J. Fluid Mech. 1 (6), 644–666.

Sinclair, J.L., Jackson, R., 1989. Gas-particle flow in a vertical pipe with particle–particle interactions. AIChE J. 35, 1473–1486.

Soo, S.L., 1969. Pipe flow of suspensions. Appl. Sci. Res. 21, 68–84.

Tseng, A., Sahai, V., 1982. Magnetohydrodynamic flow of a suspension in pipes. Dev. Theoret. Appl. Mech. 11, 397.

Tsuo, Y.P., Gidaspow, D., 1990. Computation of flow patterns in circulating fluidized beds. AIChE J. 36, 888–896.

White, F., 1991. Viscous Fluid Flow, 2nd ed. McGraw-Hill, New York.